



Reprint

Benzodithiophene-*S,S*-tetraoxide (BDTT) as an Acceptor Towards Donor-Acceptor (D-A)-Type Semiconducting Electropolymers

Tharindu A. Ranathunge,^[a] L. P. Tharika Nirmani,^[b] Toby L. Nelson,^[b] and Davita L. Watkins*^[a]

This study introduces a benzodithiophene-*S,S*-tetraoxide (BDTT) monomer as an acceptor and 3,4-ethylenedioxythiophene flanked thiophene (TEDOT₂) and terthiophene (T₃) as donor molecules for polymer formation. The synthesis of the **poly(TEDOT₂-BDTT)** and **poly(T₃-BDTT)** copolymers was performed via a single-step monomer radical formation that is typically associated with electropolymerization methods. The electropolymerization is controlled by using a suitable monomer stoichiometric ratio that enables the deposition of copolymer

thin films on the working electrode. Resultant copolymers were investigated by electrochemical analysis and their electronic properties are discussed in detail. A low average electron transport resistance of 16.5 Ω was found for **poly(TEDOT₂-BDTT)**, indicating excellent conductive behavior. Solid-state absorbance and emission studies of the copolymers show visible to near-infrared spectral activity. Results support an effective strategy towards highly efficient electronically conducting polymers (ECPs) based on a unique BDTT monomer.

1. Introduction

Recent developments in conducting polymers have enabled their use in diverse industrial applications such as lithium-ion batteries,^[1] organic photovoltaics,^[2] organic field-effect transistors (OFET),^[3] and NIR polymer probes.^[4,5] In part, the donor-acceptor (D-A) design is an effective strategy to tune the optical band gap of a material. Such molecular designs can influence the bandgap difference between electron-rich donors and electron-poor acceptors, with the development of new acceptor moieties affecting the most change in regards to the optical properties.^[6–9] Their compositions have played crucial roles in molecular planarity and crystallinity, power conversion efficiency,^[10,11] photoluminescence,^[12] and thermal-mechanical stability.^[13,14] However, reports have shown challenges associated with this strategy when applied to the systematic optimization of conjugated polymers.

Throughout decades of work, different types of synthetic approaches were implemented to afford these D–A polymers. The use of direct arylation,^[15–17] palladium cross-coupling,^[18,19] organometallic polycondensation,^[20,21] and electropolymerization^[22,23] as synthetic methods have all been shown to provide these polymers effectively. Among all of these methods, however, electropolymerization is the most

straightforward, efficient, and environmentally friendly technique.

There are several examples of applying electropolymerization to form D-A conjugated polymers. Malik et al. developed an electrochromic D-A-D polymer consist of triphenylamine (TPA) as a donor and isonaphthalene diimide as an acceptor.^[24] Rybakiewicz and co-workers electro-synthesized a naphthalene diimide core-functionalized with 1,4-phenylene functionalized carbazole to obtain donor- π -linker-acceptor- π -linker-donor (D- π -A- π -D) type polymers.^[25] In another attempt, Lu and co-workers developed two donor-acceptor type pyrazine-EDOT hybrid polymers.^[26] We, too, have shown the advantages of electropolymerization to make D-A polymers. These studies consist of benzothiadiazole (BTD),^[27] terthiophene (T₃) incorporated as a donor with thienothiadiazole-bisthiophene (TTDT₂), diketopyrrolopyrrole-bisfuran (DPPF₂) and diketopyrrolopyrrole-bisthiophene (DPPT₂) and isoindigo^[26] employed as acceptors.^[27,28]

Herein, we introduce benzodithiophene-*S,S*-tetraoxide (BDTT) as an acceptor for polymerization of p-type materials for application in optoelectronic devices. BDTT has seen limited utility as a building block for conjugated materials due to difficulties in chemical functionalization and low yields.^[29,30] Despite its limited synthetic accessibility, BDTT was previously implemented in direct arylation studies for regioselective functionalization and proven as an efficient acceptor in D-A type molecular strategy for n-type materials.^[30,31] Interestingly, its electrochemical synthesis and conductivity have not been studied. We, in turn, electropolymerized it using 3,4-ethylenedioxythiophene flanked thiophene (TEDOT₂) and T₃ as our donor monomer. These latter molecules act as radical initiators, π -linker, and donors simultaneously. The monomeric units, and their four resulting polymers are illustrated in Figure 1, **poly(T₃)**, **poly(TEDOT₂)**, **poly(T₃-BDTT)**, and **poly(TEDOT₂-BDTT)**, respectively. Electropolymerization yields conducting polymers where

[a] T. A. Ranathunge, Prof. D. L. Watkins
Department of Chemistry and Biochemistry
University of Mississippi
University, Mississippi, MS 38677–1848, USA
E-mail: dwwatkins@olemiss.edu

[b] L. P. T. Nirmani, Prof. T. L. Nelson
Department of Chemistry
Oklahoma State University
Stillwater, OK 74078, USA

 Supporting information for this article is available on the WWW under <https://doi.org/10.1002/celec.202100219>

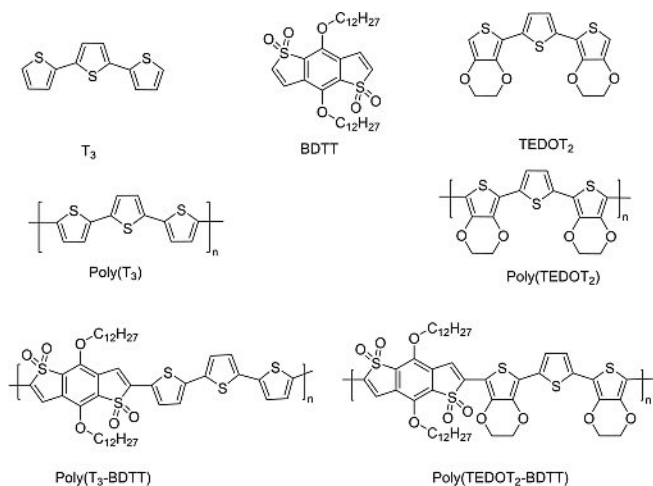


Figure 1. Monomers and respective hypothesized structures of the polymers formed via electropolymerization.

impedance spectroscopy is used to measure the electrical conductivity of the polymers. A dual rail-transmission circuit is used to rationalize the conductivities obtain in solid-state thin films via Nyquist plots. Optical properties were studied to demonstrate the absorbance, emission, and reflectance of the solid-state polymeric material. Here we summarize our results to showcase the application of BDTT as a promising acceptor moiety for the realization of high-performing conductive materials.

2. Results and Discussion

2.1. Electro-copolymerization

The initial investigation consists of introducing BDTT as an acceptor for D-A type polymer via electropolymerization. Additional details regarding monomer synthesis, electrochemical and photophysical characterization are available in the Supporting Information (Figure S1–S11). The electrochemical activity of BDTT from selected chemical potentials was scanned through ranges of -1.0 V to $+1.0$ V, -2.0 V to $+2.0$ V, and -2.0 V to $+3.0$ V and their cyclic voltammograms (CVs) are shown in Figures S9–S11. There were two oxidation onsets observed at $+0.355$ V, and $+1.069$ V that are shown in Figure S12 in the range from 0 V to $+1.2$ V. The polymerization attempt was conducted as shown in Figure S13 for this particular potential range. The CVs show a random change of current densities with an increasing number of scans indicating that BDTT is incapable of polymerizing in this potential range. The non-polymerizable nature of BDTT is distinct as the monomer is unable to form a thin layer on the working electrode.

The next attempt was carried out from 0 V to $+1.8$ V as shown in Figures S14–S15 and illustrate the origin of two oxidation peaks at $+1.195$ V and $+1.563$ V. Unlike the 0 V to $+1.2$ V range, the reduction peaks visible in this range appear at $+0.350$ V and $+1.350$ V. However, the polymerization at-

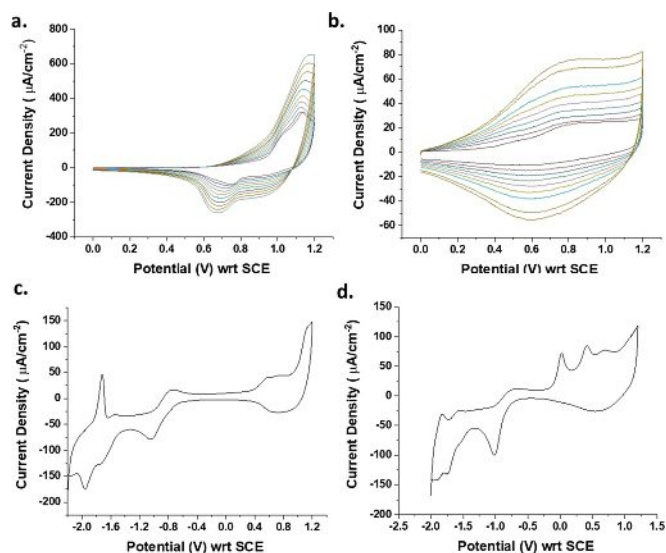


Figure 2. CVs representing electropolymerization of a) BDTT and T_3 and b) BDTT and $TEDOT_2$ monomer mixtures leading to **poly(T_3 -BDIT)** and **poly($TEDOT_2$ -BDIT)**, respectively, on a GC electrode surface. CVs of **poly(T_3 -BDIT)** and **poly($TEDOT_2$ -BDIT)** in neat BGE are shown in (c) and (d), respectively.

tempt ended with no result. Figure S16–S17 shows the potentials from 0 V to 2.2 V where two oxidation peaks are seen at $+1.054$ V and $+1.559$ V, respectively. As our final attempt, we extended the potential range up to 3 V to explore electrochemical trends. Note that, at higher potentials, BDTT possesses irreversible redox behavior that shows over-oxidation of the molecule.

Unlike previous ranges, the first oxidation peak is invisible due to the large current density of the second oxidation potential at $+1.560$ V (Figure S18–S19). These plots show random current density patterns with respect to the increment of the number of scans. Still, however, no homopolymer is detected as corresponding polymerization curves (Figures S13, S15, S17, and S19) show the inability of these oxidation potentials to produce a sole polymer made of BDTT alone even using a potentiodynamic range. Although BDTT was unable to homopolymerize, it can still be copolymerized using a radical initiator. Similar to previous studies using diketopyrrolopyrrole (DPP) and thienothiadiazole (TTD), BDTT is electrochemically active and these oxidation values can be used to link radical donors at each end of the thiophene units.^[27,28]

Acknowledging the inability of BDTT to form a homopolymer, we then introduced a donor molecule as an initiator for the polymerization.^[25–27] BDTT was copolymerized separately with either T_3 or $TEDOT_2$ under mild oxidative electrochemical conditions from 0 to $+1.2$ V to result in two different corresponding copolymers, **poly(T_3 -BDIT)**, and **poly($TEDOT_2$ -BDIT)**. Electropolymerization with the two donor molecules is evident via a successive increase in currents in repetitive CVs and concomitant deposition of polymer films on the working electrode (WE) surface. Figures 2a and b show successive CVs for the formation of the two copolymers of BDTT with T_3 and $TEDOT_2$, respectively. After the polymers were formed on the

WE surface, they were rinsed with acetone to remove small soluble organic impurities. CVs run in argon purged background electrolyte (BGE) solution without monomers are shown in Figures 2c and d. Additional details of the electropolymerization for T_3 or $TEDOT_2$ with BDTT are given in the Supporting Information.

It is important to note that **poly(T_3 -BDTT)** and **poly($TEDOT_2$ -BDTT)** exhibit different redox characteristics from that of T_3 and $TEDOT_2$ homopolymers, **poly(T_3)** and **poly($TEDOT_2$)**. The corresponding CVs for **poly(T_3)** and **poly($TEDOT_2$)** are given in Figures S5–S8. The co-polymerization was achieved with 10 repetitive scans from 0 V to +1.2 V versus SCE with a potential scan rate of 100 mVs⁻¹. Such differences support the ability of T_3 and $TEDOT_2$ to act as both polymerization initiators and linkers between the BDTT. Details of the electropolymerization for T_3 or $TEDOT_2$ with BDTT are given in the Supporting Information.

The process of electropolymerization to yield **poly(T_3)** is well-established and is used to rule out the possibility of forming **poly(T_3)**, alone.^[27] **poly(T_3)** has two-electron transfer onsets, which resemble two types of radical species generation. The first electron transfer at +0.639 V corresponds to the formation of the mono-radical cation ($T_3^{\cdot+}$). The second one appears at +0.972 V corresponds to the dication radical generated from (T_3^{2+}). Polymerization can occur beyond the upper limit of the first oxidation potential. However, the rate determined at the second oxidation step is higher than the first oxidation step, as appeared in our previous work.^[27] This phenomenon explains the ability of dication species to afford successive monomer units attached at both terminal thiophenes of T_3 while mono-radicals can add one at a time sequentially. Alternatively, polymerization of $TEDOT_2$ carried out at the anodic potential of +1.2 V (Figure S7) shows the highest current density of 93 $\mu\text{A}/\text{cm}^2$.

Electrochemical activity from 0 V to +1.2 V of **poly($TEDOT_2$)** shows (Figure S8) two oxidation onsets due to a radical formation similar to **poly(T_3)**. The first peak appearing at +0.355 V is due to the cationic radical formation of the polymer propagation step and corresponds to **poly(EDOT-T-EDOT⁺)**. A second peak at +1.069 V is due to the formation of a dication radical, **poly(⁺EDOT-T-EDOT⁺)**. $TEDOT_2$ polymerizes at both +0.8 V and +1.0 V. A poor rate of deposition is noticed at these two potentials, presumably due to the presence of single or multiple mono-radical cations instead of multiple diradical cation species. Therefore, +1.2 V potential was chosen to obtain a higher rate of deposition and also to study the presence of both oxidation potentials in the resulting polymer. The resultant polymer shows an excellent electrochemical profile in both reduction and oxidation potentials from -1.5 V to +1.2 V (Figure S8). Similar to what we have seen for T_3 , this electrochemical profile highlights the prospect of using $TEDOT_2$ as a polymer initiator for future co-polymerization attempts with other types of monomers.^[27]

Noting the electrochemical properties of **poly(T_3)** and **poly($TEDOT_2$)**, we can rationalize their use as radical initiators with BDTT to form copolymers under a constant potentiodynamic environment. Firstly, we note that to co-polymerize BDTT with

both T_3 or $TEDOT_2$, it is unfavorable to make copolymers at potentials between the two oxidation potential onsets of each polymer initiator. Surpassing both second oxidation potentials is a necessity to achieve successful copolymers in both cases. As our speculation for the T_3 initiator consists of diradical cation, $T_3^{\cdot+}$ is inducing the chronological oxidation of two sulfothiophene(ST) units at the terminal ends of the benzo unit(BZ) in BDTT. Therefore, the propagation step results in the formation of a -ST-BZ-ST- T_3 -ST-BZ-ST- sequence. On the other hand, the $TEDOT_2$ initiator consists of a diradical cation $^+\text{EDOT-T-EDOT}^+$ which works as the polymer initiator to oxidize the sulfo-thiophene terminals. This, of course, leads to the formation of a -ST-BZ-ST-EDOT-T-EDOT-ST-BZ-ST- sequence for linking EDOT terminals to BDTT. These units are required for further propagation of both types of polymerization reactions. This would lead to the formation of alternating copolymers of **T_3 -BDTT** and **$TEDOT_2$ -BDTT** if only both T_3 and $TEDOT_2$ are used to couple the other monomer units.

Comparatively, the electrochemical kinetics of **poly(T_3 -BDTT)** and **poly($TEDOT_2$ -BDTT)** were similar at comparable current density ranges at +150 $\mu\text{A}/\text{cm}^2$ and -200 $\mu\text{A}/\text{cm}^2$ (Figure 2c and d). The polymer propagation steps for both **poly(T_3 -BDTT)** and **poly($TEDOT_2$ -BDTT)** show an increase in current density. However, at oxidative potentials, a noticeably higher current density discrepancy was observed for **poly(T_3 -BDTT)** due to faster polymerization kinetics relative to **poly($TEDOT_2$ -BDTT)**.^[27,32,33] As shown in Figure 2c and d, anodic peak current densities are observed for **poly(T_3 -BDTT)** at 0.57 V ($J=38 \mu\text{A}/\text{cm}^2$) and 0.74 V ($J=45 \mu\text{A}/\text{cm}^2$). For **poly($TEDOT_2$ -BDTT)**, the anodic peak current densities are observed at 0.02 V ($J=72 \mu\text{A}/\text{cm}^2$), 0.42 V ($J=85 \mu\text{A}/\text{cm}^2$), and 0.7 V ($J=77 \mu\text{A}/\text{cm}^2$). The higher current densities in **poly($TEDOT_2$ -BDTT)** are a result of faster polymerization rates for the EDOT initiator. This result is leads to a higher deposition rate of **poly($TEDOT_2$ -BDTT)** than **poly(T_3 -BDTT)** version.

Correlation of existing polymers was analyzed by the screening-scan of polymer in neat background electrolyte as shown in Figures 3a and b. Because we could not form **poly(BDTT)**, we looked for electrochemical signatures of T_3 in **poly(T_3 -BDTT)**. The comparison between **poly(T_3)** and **poly(T_3 -BDTT)**

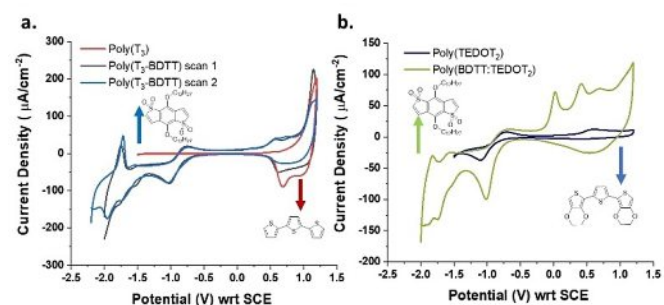


Figure 3. a) Correlation of CVs **poly(T_3)** (red line), **poly(T_3 -BDTT)** (grey line) scan from -2.0 V to +1.2 V and **poly(T_3 -BDTT)** (blue line) -2.2 V to +1.2 V. b) Correlation of CVs **poly($TEDOT_2$)** (blue line), **poly($TEDOT_2$ -BDTT)** (green line) scan from -2.0 V to +1.2 V. Arrows indicate the molecule corresponding to the particular redox background.

helps gain insight into the presence of T_3 incorporated in the polymer backbone.

Referenced via peak potentials (E_p), current density (J) and electric charge (Ah), **poly(T_3)** (Figure 3a red color) has a characteristic reduction peak centered at $E_p = +0.694$ V ($J = -27.33$ $\mu A/cm^{-2}$, $Ah = -17.39$ μC) in the potential range from -1.5 V to $+1.2$ V. In **poly(T_3 -BDTT)**, the CV from -2.0 V to $+1.2$ V (grey line) shows this peak has shifted to $+0.612$ V ($J = 50$ $\mu A/cm^{-2}$) without any interference of electronic background of BDTT monomer. This corresponding shift is due to the fingerprint electronic background achieved by the bonding of T_3 with the thiophene unit of the terminal BDTT monomer (ST- T_3 -ST). However, the scan from -2.2 V to $+1.2$ V (blue line) shows a broadening in the peak due to T_3 being bonded to thiophene dioxide (ST- T_3 -ST), hence the display of more oxidized characteristics than reductive features. These properties are due to the oxidized sulfur atoms in BDTT that are now bonded to T_3 , achieving a new chemical environment with broader kinetics.

Due to an inability to form **poly(BDTT)**, the electrochemical properties and signatures of BDTT are assessed using the monomer. Beginning with a negative potential, an excellent redox behavior for this acceptor core is seen. A significant oxidation peak is present at -0.853 V ($J = 7.8$ $\mu A/cm^{-2}$) and a return reduction peak at -1.061 V ($J = -29.6$ $\mu A/cm^{-2}$), affording the perfect reversible redox behavior caused by the acceptor core. This feature is absent in **poly(T_3)** and present in the **poly(T_3 -BDTT)** which gives direct evidence of BDTT in the copolymer. Other characteristic irreversible reduction peaks are at -1.440 V ($J = 19$ $\mu A/cm^{-2}$) and -1.761 V ($J = 17.6$ $\mu A/cm^{-2}$) of BDTT monomer have shifted in **poly(T_3 -BDTT)** due to new bonding features. BDTT monomer features visible at the negative potentiodynamic range present after co-polymerization can be observed. The redox behavior at -1.973 V ($J = -173.3$ $\mu A/cm^{-2}$) corresponds to the reduction of BDTT monomer. Its return sweep oxidation at -1.718 V ($J = 46.91$ $\mu A/cm^{-2}$) is evidence of a new electronic environment where the BDTT monomer bonding with the T_3 linker is assigned to be $-T_3$ -ST-BZ- T_3 . The results correlate to the properties of BDTT as a strong acceptor and oxidized species (or bearing oxidized sulfur atoms).

The electrochemical signature of **TEDOT₂** was analyzed in a similar method (Figure 3b) by plotting **poly(TEDOT₂)** with **poly(TEDOT₂-BDTT)**. **Poly(TEDOT₂)** (Figure 3b blue color) shows two oxidation potentials that characteristically irreversible centered at $E_p = +0.075$ V ($J = 12$ $\mu A/cm^{-2}$), and $+0.680$ V ($J = 77$ $\mu A/cm^{-2}$) show the peak shift without any interference of electronic background of the BDTT monomer. Noticeably, two irreversible oxidation peaks appear at the lower positive regime in **poly(TEDOT₂-BDTT)**. The first peak at $+0.014$ V ($J = 71.4$ $\mu A/cm^{-2}$) corresponds to the BDTT monomer. The second oxidation potential at $+0.420$ V ($J = 85$ $\mu A/cm^{-2}$) also corresponds to the BDTT monomer (Figure S12) that has shifted from $+0.355$ V.

Further evidence for the presence of BDTT can be validated by assessing the negative regime. A reduction peak at -1.031 V ($J = -98.3$ $\mu A/cm^{-2}$) and return sweep oxidation peak present at -0.732 V ($J = 7.7$ $\mu A/cm^{-2}$) expose a quasi-reversible redox

behavior that is caused by both the BDTT acceptor core (BZ) and **TEDOT₂** monomers. The redox behavior of BDTT can be noticed by looking at deeper potentials. Reduction peak at -1.792 V ($J = -132$ $\mu A/cm^{-2}$) and return sweep oxidation at -1.573 V ($J = -25$ $\mu A/cm^{-2}$) indicates a new bonding environment between monomers EDOT and BDTT. These bonds can be assigned to the $-EDOT$ -ST-BZ-ST-EDOT- sequence and show the dominating redox behavior of BDTT now present in the polymer backbone. In addition, reduction peak at -1.945 V ($J = -142$ $\mu A/cm^{-2}$) and return sweep oxidation peak at -1.829 V ($J = -30.5$ $\mu A/cm^{-2}$) is due to the acceptor core.

Current differences between the two CVs indicate that **poly(TEDOT₂-BDTT)** has faster electrochemical polymerization kinetics than **poly(TEDOT₂)**. The presence of electron-rich acceptor core has provided additional indirect evidence of copolymerization. The trends in current and charge values for redox peaks indicate that the two monomer units are most likely 1:1 and that **poly(T_3 -BDTT)** and **poly(TEDOT₂-BDTT)** both exhibit intriguing electrical properties.

2.2. Electrical Properties

AC impedance spectroscopy is an essential tool to characterize electronically conducting polymers (ECPs). Note that there is a difference in the bandgap between the monomers and their resulting polymers. Before the electrosynthesis, these individual monomers have a higher bandgap. After electropolymerization, the resulting polymer achieves a lower bandgap. This decrease in band gap yields a condition where the conduction band (CB) and valence band (VB) of the polymer can exchange electrons. Thus, the resulting polymers, **poly(T_3 -BDTT)** and **poly(TEDOT₂-BDTT)**, act as semiconducting materials relative to their individual monomers. The significant electronic features observed in each polymer are due to conjugated double bonds along the polymer backbone. This includes strongly localized σ -bonds and weakly localized π -bonds. The conductivity is dependent on the doping of the polymer. Herein, the polymers are positively-doped with cations (p-dope status) upon electropolymerization at positive oxidation potentials. The polymer dopants consist of charged moieties that transfer electrons and holes subsequently. The redox behavior of the polymer is comprised of charge carriers such as polarons (radical cations), and bipolarons (dications).^[33]

Impedance spectra of copolymers were recorded for both copolymers starting from -1.0 V to $+1.0$ V with a recording sequence of 0.2 V throughout negative and positive potentials. These plots were analyzed by the dual-rail transmission line circuit model proposed to determine the electrical properties for ECPs.^[34-37] All of the impedance data was converted to conducting properties and is shown in Table 1 and 2. The dual rail transmission line circuit and simplified equivalent circuit models are shown in the Supporting Information (Figure S20).

The resulting Nyquist plots are reported in the Supporting Information (Figures S21-S26). Nyquist and Bode plots were recorded for **poly(TEDOT₂)**, **poly(T_3 -BDTT)**, and **poly(TEDOT₂-**

Table 1. Electrical properties of poly(T₃-BDTT) were obtained from fitting AC impedance Nyquist plots to the equivalent circuit as shown in Figures S21–S22 (Supporting Information).

Poly(T ₃ -BDTT) E [V]	R _s ^[a] [Ω]	R _e ^[b] [Ω]	C _d ^[c] [μF]	W ^[d] [μΩ]	C ^[e] [μF]
−2.0	57.66	94.56	3.356	110.4	2.976
−1.8	31.34	35.43	4.246	61.34	3.298
−1.6	45.56	867.7	3.566	90.56	3.134
−1.4	42.48	5687	3.173	465.4	3.294
−1.2	47.13	185.4	3.295	103.7	2.856
−1.0	35.95	238.0	3.261	62.48	3.230
−0.8	37.20	173.7	3.191	98.52	3.261
−0.6	41.90	585.4	3.295	103.7	2.856
−0.4	45.30	648.7	3.295	133.9	2.846
−0.2	42.66	363.1	3.381	39.42	2.937
0.0	43.84	73.56	3.346	177.4	3.346
+0.2	42.29	825.0	9.252	120.1	2.235
+0.4	42.75	639.0	3.210	55.81	2.426
+0.6	40.48	493.0	3.148	34.47	3.573
+0.8	43.21	126.5	3.173	36.81	3.875
+1.0	45.44	129.2	4.844	47.52	3.650

[a] R_s: series resistance of the cell. [b] R_e: resistance for electron transport along the polymer backbone. [c] C_d: double layer capacitance between polymer-electrolyte interface. [d] W: Warburg impedance for ingress and egress of counter ions by diffusion. [e] C: capacitance of the high frequency pure capacitive regime.

Table 2. Electrical properties of poly(TEDOT₂-BDTT) obtained from fitting AC impedance Nyquist plots to the equivalent circuit, as explained in Figures S23–S24 (Supporting Information).

Poly(TEDOT ₂ -BDTT) E [V]	R _s ^[a] [Ω]	R _e ^[b] [Ω]	C _d ^[c] [μF]	W ^[d] [μΩ]	C ^[e] [μF]
−2.0	8.680	134.2	0.234	31.45	1.112
−1.8	8.350	245.5	0.275	35.57	1.346
−1.6	8.120	536.1	0.257	47.56	1.422
−1.4	9.160	1112	0.928	36.40	1.514
−1.2	3.810	735.0	0.374	40.17	1.481
−1.0	2.630	138.7	0.071	22.48	1.45
−0.8	8.580	535.5	0.57	63.79	1.076
−0.6	7.180	935.5	0.899	63.79	1.076
−0.4	7.330	636.7	0.57	63.79	1.066
−0.2	9.340	418.1	0.193	6.42	1.157
0.0	10.52	28.56	0.156	77.40	1.566
+0.2	8.970	224.7	0.812	60.09	0.455
+0.4	9.430	239.2	0.021	55.81	0.646
+0.6	7.160	93.83	0.0044	34.47	1.793
+0.8	9.890	16.55	0.0292	36.81	3.095
+1.0	12.12	19.28	1.304	47.52	1.279

[a] R_s: series resistance of the cell. [b] R_e: resistance for electron transport along the polymer backbone. [c] C_d: double layer capacitance between polymer-electrolyte interface. [d] W: Warburg impedance for ingress and egress of counter ions by diffusion. [e] C: capacitance of the high frequency pure capacitive regime.

BDTT). AC impedance data for poly(T₃) is available from previous work.^[27]

In general, poly(T₃-BDTT) and poly(TEDOT₂-BDTT) exhibit similar conducting patterns throughout the potential range but poly(TEDOT₂) and poly(T₃) slightly differ. Table S3 summarizes the conducting behavior of the latter two polymers. The poly(TEDOT₂) and poly(T₃) display insulating properties in the negative regime. This is also confirmed by the higher current densities observed in the positive regime of both poly(TEDOT₂) and poly(T₃). For the copolymers, poly(TEDOT₂-BDTT) shows higher conductivity values than poly(T₃-BDTT) due to a more polarized polymer backbone extended from the EDOT moieties. Conductivity is relatively higher in this polymer at both negative

and positive potentials because of the more polarized polymer backbone in the presence of oxidized sulfur.

Consequently, electron density from T₃ and TEDOT₂ on both sides of BDTT tends to polarize the polymer backbone more effectively than when either of the donors presents on their own. For poly(T₃-BDTT), the average electron transport resistance (R_e) was 697.8 Ω throughout −2.0 V to +1.0 V potential series (Table 1). Higher conductivity trends can be observed at −2.0 V, −1.8 V, −1.2 V, −1.0 V, −0.8 V, and at zero bias potentials of an average value of R_e 133.45 Ω. Even pristine conductance at zero potential indicates that the polymer itself has intrinsic electrical properties due to effective polarization. Similar to poly(T₃) at the +0.8 and +1.0 V positive potentials, poly(T₃-BDTT) R_e-value has an average of 127.9 Ω. Further

insights into the semiconductive behavior of **poly(T₃-BDTT)** is observed by the Nyquist plots located in the Supporting Information (Figure S21–22). The double-layer capacitance (C_d) values are low (from 2.2 to 3.87 μF) in the potential range between -2.0 V and $+1.0\text{ V}$ with an average value of 3.11 μF . This independent nature of capacitance of applied potential range provides direct evidence for an ECP.

Warburg impedance (W) shows the analogous behavior range of 35 $\mu\Omega$ to 135 $\mu\Omega$ in the potential range of -2.0 V and $+1.0\text{ V}$ also acts as an independent variable. The reversible redox nature of **poly(T₃-BDTT)** at negative potentials is the reason for its excellent conducting nature. Once again, this is due to the presence of the BDTT moiety within the polymer framework.

The electrical properties of **poly(TEDOT₂-BDTT)** are shown in Table 2. **Poly(TEDOT₂-BDTT)** has, on average, considerably lower resistance values (378 Ω) for electron transport (R_e) than **poly(T₃-BDTT)**. Similarly, both polymers show excellent conductance at both negative and positive regimes. Noticeably, **poly(TEDOT₂-BDTT)** at -2.0 V , -1.8 V , -1.0 V , and zero bias potentials have an average R_e of 193 Ω . This is a lower conductivity with comparison to **poly(T₃-BDTT)**. At zero potential, both **poly(T₃-BDTT)** and **poly(TEDOT₂-BDTT)** show low resistance values indicating that the polymer has intrinsic conducting properties. **Poly(TEDOT₂-BDTT)** shows excellent conductivity at positive potentials due to the heavily p-doped nature of the EDOT moieties. This is further confirmed by the large redox band in the positive potential regime of the polymer CV. **Poly(TEDOT₂)** has similar electronic properties at the positive potentials as shown in Table S3. In contrast, **poly(TEDOT₂-BDTT)** is drastically nonconducting throughout the negative potential regime exhibiting a high electron-transport resistance between -0.6 V and -1.4 V . This is similar to the electronic performance of **poly(T₃)**, which also possessed a lack of conductivity at negative potentials. Unlike **poly(T₃)**, **poly(TEDOT₂)** shows excellent conductivity from -0.4 V to $+1.0\text{ V}$ with an average electron transport resistance of 117.4 Ω . **Poly(TEDOT₂-BDTT)** shows conductivity from $+0.2\text{ V}$ to $+1.0\text{ V}$ with an average of 118.7 Ω . This reflects the corresponding electronic behavior of **poly(TEDOT₂)** dominant as TEDOT₂ monomers entangled in the polymer backbone. However, at higher p-doped potentials $+0.8\text{ V}$ to $+1.0\text{ V}$, **poly(TEDOT₂-BDTT)** shows an average electron transport resistance of 17.9 Ω lower than **poly(TEDOT₂)**, which is 60.1 Ω .

Relative to conventional polymers with similar molecular frameworks (Table S4), the average R_e (Ω) indicates that conductivity increases in the positive potential of EDOT based polymers. For **poly(TEDOT₂-BDTT)**, the p-doped electron transport resistance at $+0.8\text{ V}$ is 16.6 Ω and the de-doped resistance is 28.6 Ω , a relatively high conductance for a sulfur-based polymer.

Further insight into the semiconductive behavior of **poly(T₃-BDTT)** and **poly(TEDOT₂)** are seen in their Nyquist plots in the Supporting Information (Figure S23–26). The average double-layer capacitance (C_d) values for **poly(TEDOT₂-BDTT)** and **poly(TEDOT₂)** are 0.417 μF and 2469 μF , respectively. Warburg impedance (W) shows a trend that correlates with this behavior

range from 6.4 $\mu\Omega$ to 63.7 $\mu\Omega$ from -2.0 V to $+1.0\text{ V}$ in **poly(TEDOT₂-BDTT)**. Results indicate that **poly(TEDOT₂-BDTT)** shows better electronic properties than **poly(T₃-BDTT)** and all the homopolymers in this study.

2.3. Optical Properties

The mechanistic p-doping of both **poly(T₃-BDTT)** and **poly(TEDOT₂-BDTT)** respectively consists of two steps. First, the formation of mono cationic polaron state and second, a dication-bipolaron state. In these states, double bonds are forming between the D-A units that lead to different bonding patterns in the ground and excited-state resulting in the formation of various low energy optical bands close to NIR-I (650 nm–950 nm), NIR-II-a (950 nm–1450 nm), and NIR-II-b (1450 nm–2500 nm).^[38]

To confirm these optical properties, copolymers were formed using 50 successive scans to obtain a thin polymer film deposited on FTO glass. Both copolymers display optical absorbances throughout the visible to NIR-II region (Figure 4a). In the solid-state, p-doped **poly(TEDOT₂-BDTT)** shows multiple spectral maxima throughout 400 nm to 2000 nm. The absorbance at 477 nm is indicative of a $\pi \rightarrow \pi^*$ transition.

Poly(T₃-BDTT) is excited at 535 nm and shows a traditional $\pi^* \rightarrow \pi$ transition at 657 nm (Figure 4b). This indicates that even in the solid-state this material can emit photons successively.^[39] **Poly(TEDOT₂-BDTT)** was excited at 477 nm and its emission profile shows a broadband spectrum due to the extended charge transfer system formed by the copolymer. **Poly(TEDOT₂-BDTT)** shows the highest intensity maximum at 576 nm. These characteristics are widely useful in many applications that are related to the design of NIR-optoelectronic materials.

The optical band gap of thin films is calculated experimentally using Tauc plot analysis.^[40] According to the Tauc plot

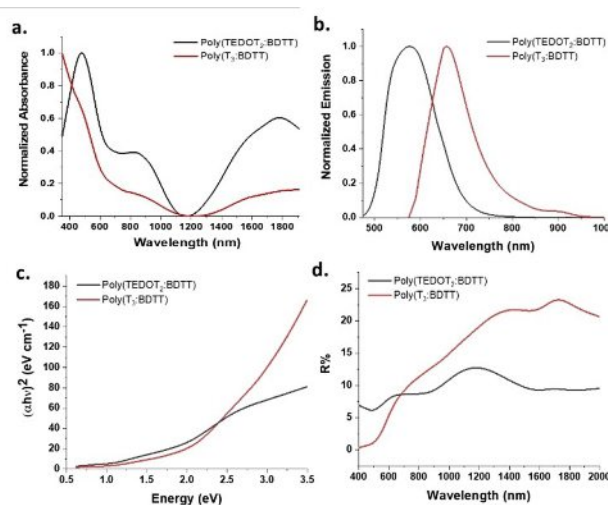


Figure 4. Optical properties of a) solid-state thin-film absorbance of copolymers, b) solid-state emission of copolymers, c) Tauc plot of solid-state copolymers, and d) reflectance (%) dispersion in the visible to near IR spectral range of polymer thin films.

(Figure 4c), the bandgap is reported 1.575 eV for **poly(TEDOT₂-BDTT)**. Due to the doped states (Figure S27) polaron band appears at 0.946 eV and the bipolaron band appears at 0.632 eV. Similarly, **poly(T₃-BDTT)** shows $\pi \rightarrow \pi^*$ transition and $n \rightarrow \pi^*$ transitions. In the visible range, these properties are inconspicuous, presumably due to the solid-state packing order.^[41] The optical band gap obtained from the Tauc plot is 2.302 eV which is higher than the former copolymer. The corresponding (Figure S28) polaron band appeared at 1.824 eV and the bipolaron band appeared at 0.812 eV. Comparative band gap analysis is shown in Table S5.

Reflectance is directly correlated to the thin film thickness of the material.^[42] Additionally, absorbance and reflectance are related. In turn, we investigated the percentage reflectance from 400 nm to 2000 nm to understand the interesting optical properties for each polymer that are presumably due to film thickness. **Poly(TEDOT₂-BDTT)** shows low reflectance range of 6% to 12% where **poly(T₃-BDTT)** shows higher reflectance range 0.2 to 22.25%. This is due to the thickness of the deposited thin layer for **poly(TEDOT₂-BDTT)** is higher than **poly(T₃-BDTT)**. In addition, it provides direct evidence for the higher kinetics of **poly(TEDOT₂-BDTT)** in the polymer propagation step. Comparatively, this leads **poly(TEDOT₂-BDTT)** to show electronic properties, lower bandgap, and broader emission profile. Such results support that both copolymers are suitable for NIR triggered optoelectronic material with **poly(TEDOT₂-BDTT)** being the most promising candidate for further application.

3. Conclusions

In summary, BDTT monomer is utilized as an acceptor towards designing D-A type polymers. The study implemented a single step radically associated electropolymerization to obtain copolymers. Two copolymers **poly(T₃-BDTT)** and **poly(TEDOT₂-BDTT)** were investigated and electrochemical evidence aided in rationalizing the structural outcome of the electrosynthesis. Studies indicate that TEDOT₂-BDTT monomer mixtures lead to faster polymerization kinetics relative to T₃-BDTT based polymers. The resulting polymers show excellent conductivities compared to their building blocks with the lowest electron transport resistance reported of 16.5 Ω for **poly(TEDOT₂-BDTT)**. Further investigation shows that the polymers exhibit absorbance throughout the visible to the NIR region with both copolymers showing high-intensity fluorescence from 500 nm to 1000 nm. These results show that BDTT can be used as an electron acceptor in electro-copolymerization to yield promising NIR optoelectronic materials.

Experimental Section

Materials

All reagents were obtained from commercial vendors and used as received unless otherwise stated. The synthetic pathways for BDTT,

T₃, and TEDOT₂ monomers were adopted from previously reported literature^[27,30,31,43] and outlined in the Supporting Information (Figure S1–S3). The Photophysical properties of BDTT is reported in Supporting Information (Figure S4).

Electropolymerization

The one-step electro-copolymerization method was implemented in this study based on the stoichiometric ratios of the monomers as previously reported.^[16] In brief, monomer mixtures of BDTT and T₃ for **poly(T₃-BDTT)** or BDTT and TEDOT₂ for **poly(TEDOT₂-BDTT)** were dissolved in 10 mL of acetonitrile such that each monomer is in 1 mmol dm⁻³ concentration within the solution. (Calculated amounts are presented in Tables S1 and S2). Background electrolyte was prepared using tetrabutylammonium hexafluorophosphate (0.1 mol dm⁻³ concentration).

All the electrochemical studies were performed in a one-compartment cell containing three electrodes with a glassy carbon (GC) or fluorine-doped tin oxide (FTO) working electrode (WE), a saturated calomel electrode (SCE) as the reference electrode (RE), and a Pt-wire counter electrode (CE). All potentials are measured against SCE unless otherwise stated. In each case, the solution was degassed by purging with high purity argon gas for 20 minutes and a slow flow of argon was maintained above the solution to prevent re-entry of air. Electro-copolymerization was performed via 10 repetitive CV cycles by selecting a potential range between 0.0 V and +1.2 V to prevent over-oxidation of polymers. The polymer films obtained on the WE surface were washed with acetone to remove any small organic residue and CV and AC-impedance characteristics were recorded in argon purged neat BGE without monomers. CVs were recorded in the potential range within -2.2 V to +1.2 V to include all redox peaks of the copolymers and a scan rate of 100 mV s⁻¹ was used unless otherwise indicated. Nyquist and Bode plots of AC impedance characteristics were recorded in the frequency range from 0.1 Hz to 1 MHz at several selected DC potential bias values in the above potential range which contained all the information of the electrochemical system being investigated. Electrochemical characterization for **poly(T₃)**, **poly(TEDOT₂)** and BDTT is shown in the Supporting Information (Figure S5–S11).

Photophysical properties

Samples were deposited and studied on fluorine-doped tin oxide (FTO) substrates. To remove any residual solvents, the samples were cleaned with acetone and dried in a vacuum oven at 50 °C before obtaining ultraviolet-visible-near infrared-short wavelength infrared (UV-Vis-NIR-SWIR) spectra. UV-Vis-NIR-SWIR spectra were measured with a Cary 5000 spectrophotometer on the samples deposited on FTO substrates. Emission was measured using the Horiba FluoroMax fluorescence spectrophotometer of tunable excitation wavelength from 350 nm to 1000 nm range using a 5 nm slit for the solid-state compartment. Excitation wavelengths were chosen using the absorption maximum of solid-state.

Acknowledgements

The authors appreciate financial support of this work from the National Science Foundation under Grant Number NSF OIA-1757220.

Conflict of Interest

The authors declare no conflict of interest.

Keywords: thiophene · copolymers · electropolymerization · impedance · near-infrared

- [1] W. Shen, K. Li, Y. Lv, T. Xu, D. Wei, Z. Liu, *Adv. Energy Mater.* **2020**, *10*, 1904281.
- [2] Z. Ding, R. Zhao, Y. Yu, J. Liu, *J. Mater. Chem. A* **2019**, *7*, 26533.
- [3] A. W. Lang, Y. Li, M. De Keersmaecker, D. E. Shen, A. M. Österholm, L. Berglund, J. R. Reynolds, *ChemSusChem* **2018**, *11*, 854.
- [4] J. Xu, L. Yu, Z. Sun, T. Li, H. Chen, W. Yang, *Org. Electron.* **2020**, *84*, 105785.
- [5] M. J. Ford, M. Wang, K. C. Bustillo, J. Yuan, T.-Q. Nguyen, G. C. Bazan, *ACS Nano* **2018**, *12*, 7134.
- [6] K. Müllen, W. Pisula, *J. Am. Chem. Soc.* **2015**, *137*, 9503.
- [7] M. Kim, S. U. Ryu, S. A. Park, K. Choi, T. Kim, D. Chung, T. Park, *Adv. Funct. Mater.* **2020**, *30*, 1904545.
- [8] K. Mahesh, S. Karpagam, K. Pandian, *Top. Curr. Chem.* **2019**, *377*, 12.
- [9] Y. Han, Z. Xing, P. Ma, S. Li, C. Wang, Z. Jiang, Z. Chen, *ACS Appl. Mater. Interfaces* **2020**, *12*, 7529.
- [10] C. L. Chochos, R. Singh, V. G. Gregoriou, M. Kim, A. Katsouras, E. Serpetzoglou, I. Konidakis, E. Stratakis, K. Cho, A. Avgeropoulos, *ACS Appl. Mater. Interfaces* **2018**, *10*, 10236.
- [11] C. L. Chochos, A. S. Kalogirou, T. Ye, E. Tatsi, A. Katsouras, G. A. Zissimou, V. G. Gregoriou, A. Avgeropoulos, P. A. Koutentis, *J. Mater. Chem.* **2018**, *6*, 3658.
- [12] Y. Qu, P. Pander, O. Vybornyi, M. Vasylieva, R. Guillot, F. Miomandre, F. B. Dias, P. Skabara, P. Data, G. Clavier, P. Audebert, *J. Org. Chem.* **2020**, *85*, 3407.
- [13] X. Gao, J. Gao, Z. Xue, H. Wang, J. Wang, Y. Cheng, Z. Li, F. Zhu, S. Huettner, H. Li, Y. Tao, *J. Mater. Chem.* **2019**, *7*, 10338.
- [14] R. Song, Y. Zhao, W. Li, Y. Yu, J. Sheng, Z. Li, Y. Zhang, H. Xia, W.-D. Fei, *Acta Mater.* **2019**, *181*, 200.
- [15] K. Nakabayashi, *Polym. J.* **2018**, *50*, 475.
- [16] M. Wakioka, F. Ozawa, *Asian J. Org. Chem.* **2018**, *7*, 1206.
- [17] S.-W. Chang, H. Waters, J. Kettle, Z.-R. Kuo, C.-H. Li, C.-Y. Yu, M. Horie, *Macromol. Rapid Commun.* **2012**, *33*, 1927.
- [18] A. K. Leone, E. A. Mueller, A. J. McNeil, *J. Am. Chem. Soc.* **2018**, *140*, 15126.
- [19] M. Gao, J. Subbiah, P. B. Geraghty, M. Chen, B. Purushothaman, X. Chen, T. Qin, D. Vak, F. H. Scholes, S. E. Watkins, M. Skidmore, G. J. Wilson, A. B. Holmes, D. J. Jones, W. W. H. Wong, *Chem. Mater.* **2016**, *28*, 3481.
- [20] "Organometallic Polycondensation for Conjugated Polymers", in *Conjugated Polymer Synthesis*, p. 1.
- [21] T. Yamamoto, T.-a. Koizumi, *Polymer* **2007**, *48*, 5449.
- [22] M. R. J. Scherer, *Double-Gyroid-Structured Functional Materials: Synthesis and Application*, "Electropolymerization of Conjugated Polymers", Springer International Publishing, Heidelberg, **2013**, p. 135.
- [23] R. J. Waltman, J. Bargon, *Can. J. Chem.* **1986**, *64*, 76.
- [24] S. Nad, S. Malik, *ChemElectroChem* **2020**, *7*, 4144.
- [25] R. Rybakiewicz, R. Ganczarczyk, M. Charyton, L. Skorka, P. Ledwon, R. Nowakowski, M. Zagorska, A. Pron, *Electrochim. Acta* **2020**, *358*, 136922.
- [26] N. E. Sparks, T. A. Ranathunge, N. H. Attanayake, P. Brodgon, J. H. Delcamp, R. M. G. Rajapakse, D. L. Watkins, *ChemElectroChem* **2020**, *7*, 3752.
- [27] T. A. Ranathunge, D. Karunathilaka, D. T. Ngo, N. H. Attanayake, P. Brodgon, J. H. Delcamp, R. M. G. Rajapakse, D. L. Watkins, *Macromol. Chem. Phys.* **2019**, *220*, 1900289.
- [28] T. A. Ranathunge, D. T. Ngo, D. Karunathilaka, N. H. Attanayake, I. Chandrasiri, P. Brodgon, J. H. Delcamp, R. M. G. Rajapakse, D. L. Watkins, *J. Mater. Chem.* **2020**, *8*, 5934.
- [29] T. M. Pappenfus, D. T. Seidenkranz, M. D. Lovander, T. L. Beck, B. J. Karels, K. Ogawa, D. E. Janzen, *J. Org. Chem.* **2014**, *79*, 9408.
- [30] S. Adhikari, Y. X. Ren, M. C. Stefan, T. L. Nelson, *Polym. Chem.* **2020**, *11*, 7421.
- [31] D. P. Khambhati, K. A. N. Sachinthan, A. L. Rheingold, T. L. Nelson, *Chem. Commun.* **2017**, *53*, 5107.
- [32] N. Elgrishi, K. J. Rountree, B. D. McCarthy, E. S. Rountree, T. T. Eisenhart, J. L. Dempsey, *J. Chem. Educ.* **2018**, *95*, 197.
- [33] T.-H. Le, Y. Kim, H. Yoon, *Polymer* **2017**, *9*, 150.
- [34] W. J. Albery, A. R. Mount, *J. Chem. Soc. Faraday Trans.* **1994**, *90*, 1115.
- [35] W. J. Albery, Z. Chen, B. R. Horrocks, A. R. Mount, P. J. Wilson, D. Bloor, A. T. Monkman, C. M. Elliott, *Faraday Discuss. Chem. Soc.* **1989**, *88*, 247.
- [36] S. J. Higgins, K. V. Lovell, R. M. Gamini Rajapakse, N. M. Walsby, *J. Mater. Chem.* **2003**, *13*, 2485.
- [37] G. Li, P. G. Pickup, *J. Phys. Chem. B* **1999**, *103*, 10143.
- [38] M. Y. Berezin, S. Achilefu, *Chem. Rev.* **2010**, *110*, 2641.
- [39] S. M. Swick, W. Zhu, M. Matta, T. J. Aldrich, A. Harbuzaru, J. T. Lopez Navarrete, R. Ponce Ortiz, K. L. Kohlstedt, G. C. Schatz, A. Facchetti, F. S. Melkonyan, T. J. Marks, *Proc. Natl. Acad. Sci. USA* **2018**, *115*, E8341.
- [40] Z. Khan, M. Khannam, N. Vinothkumar, M. De, M. Qureshi, *J. Mater. Chem.* **2012**, *22*, 12090.
- [41] S. Varghese, S. Das, *J. Phys. Chem. Lett.* **2011**, *2*, 863.
- [42] F. Houta, M. Quinten, *Optik & Photonik* **2015**, *10*, 54; *Photonik* **2015**, *10*, 54.
- [43] J. Hou, M.-H. Park, S. Zhang, Y. Yao, L.-M. Chen, J.-H. Li, Y. Yang, *Macromolecules* **2008**, *41*, 6012.

Manuscript received: February 18, 2021

Accepted manuscript online: February 23, 2021